Hindawi
Geofluids
Volume 2022, Article ID 3207575, 12 pages
https://doi.org/10.1155/2022/3207575

Research Article

X-Ray Fluorescence for Laminated Silty Shale Reservoirs in Ordos Basin, China: Implications for Lithology Identification

Wei Cheng,[1] **Hao Cheng**,[1] **Hongyan Yu**,[1] **Shaohua Zhang**,[2] **Zhenliang Wang**,[1] **Xiaolong Li**,[1] **and Lukman Johnson**[3]

[1]*State Key Laboratory of Continental Dynamics, Department of Geology, Northwest University, Xi'an, China*
[2]*Research Institute of Exploration & Development, Changqing Oilfield, PetroChina, Xi'an, China*
[3]*Department of Applied Geology, West Australian School of Mines, Curtin University, Perth, Australia*

Correspondence should be addressed to Hongyan Yu; amelia-yu@hotmail.com

Received 23 December 2021; Accepted 16 July 2022; Published 31 July 2022

Academic Editor: Mohammed Fattah

Shale lithofacies were an important key for the exploration and development of unconventional oil and gas reservoirs. Previous studies usually use logging data, X-ray diffraction analysis (XRD), and scanning electron microscopy (SEM) to identify shale lithofacies, but these methods cannot accurately and quickly identify geochemical characteristics. Portable X-ray fluorescence (XRF) analysis can identify geochemical characteristics. However, few publications reported the feasibility of XRF identifying lithology. We tested the major elements of this formation systematically by X-ray fluorescence and compared the characteristics of these elements in the silty laminated shales against the calcareous laminated shale and the argillaceous shales. We analyzed the geochemical characteristics of shale using portable XRF and proposed a method to identify argillaceous shale, silty laminated shale, and calcareous laminated shale in the Chang 7 of Well Y1 (in Xiasiwan area). Furthermore, we established a lithoface identification standard. We also found that Ca/Mg of calcareous laminated shale was the highest which indicated a dry depositional environment; in contrast, lowest Ca/Mg of silty laminated shale indicated a humid depositional environment. Argillaceous shale was deposited in a strongly reducing environment because Fe content of argillaceous shale was the highest. Finally, this criterion is tested against the data from the Well Y2, and the results are in good agreement with the thin section analysis and core data.

1. Introduction

Shale is considered a fine-grained, brittle rock that acts as an important source of petroleum [1, 2]. There are various lithofacies in shale because of changes in the depositional environment, such as silty laminated shale, calcareous layered shale, and siliceous shale. Shale was proved to be an important source rock for conventional oil, also, as source and reservoir for unconventional oil [3]. Shale is mainly composed of fine-grained quartz, clay minerals, and other minerals that include feldspar, carbonate minerals, sulfide minerals, and oxide minerals [4]. Previous published articles proposed that there were many differences in the mineral composition and elemental concentrations of different shales [5–7]. Unfortunately, no criteria for the classification of favorable shale lithofacies have been established.

Unconventional shale reservoirs contribute to an increased reservoir capacity as well as brittleness of shale units, which makes the shale reservoir conducive to formation of fractures during hydraulic fracturing as discussed [8–10]. There are many multiscale images techniques that can accurately identify shale microstructure at different scales in the past decade or so, such as 3D X-ray computed tomography (μ-CT and nano-CT) and focus ion beam/scanning electron microscopy (FIB/SEM) [11, 12]. These techniques can be combined to describe shale pore space and microfracture networks at multiple length scales due to the highly anisotropic nature of shale; however, they provide no quantitative information about fine-grained

components. Silt shale and calcareous shale were more easily fractured than argillaceous shale because of the texture. Therefore, the identification of potential silty and calcareous shale is crucial for shale oil and gas development.

The lacustrine shale of Chang 7 in the Xiasiwan area developed a large number of silty laminated, which leads to its strong heterogeneity. This lacustrine shale is composed of fine-grained quartz, clay, and other minerals such as feldspar, carbonate minerals, sulfide minerals, and oxide minerals, which proposed by previous published studies [13–17]. However, these silty laminated shales and calcareous laminated shales are usually difficult to identify by conventional tools; result in the quantification and distribution of these shales cannot be obtained through direct measurement on the core or logging data. In this study, we proposed to directly measure the elemental composition on fresh cores by XRF to study the mineralogy and geochemical characteristics. We measured the major elements of Chang 7 of Well Y1 through X-ray fluorescence (XRF) and analyzed the characteristics of the major elements in silty laminated shales, argillaceous shales, and the calcareous laminated shales. There are only four XRD samples in Well Y1, and it is not representative to discuss the relationship between a little of XRD samples and XRF based on the only experimental data. Therefore, in this study, we only described the characteristics of different lithologies and minerals. Finally, a new identification model was developed to establish a criterion for lithology identification within shale laminated, based on the elemental differences in the different shales.

2. Geological Setting

The Ordos Basin is the second largest sedimentary basin in China with an area of 25×10^4 km^2. It is located in the central part of the China and divided into six structural units, namely, the Yimeng Uplift, the Weibei Uplift, the Western Edge Thrusting Belt, the Jinxi Flexural Fold Belt, the Tianhuan Depression, and the Shanbei Slope (Figure 1).

The study area is located in the southeastern section of the Shanbei Slope, with a present dip less than 1° and no major faults or anticlines developed. The Yanchang Formation is one of the main oil-bearing series in this basin, and it is subdivided into 10 members, namely, Chang 10-Chang 1 from bottom to top [18]. The lacustrine Chang 7 Formation developed in the Late Triassic, with the shale members forming at specific phases of the basin development, showing the Chang 10 member was formed in the initial phase when the basin opened up, while Chang 9 to Chang 7 members was deposited during the basin expansion phase. Lastly, the Chang 6 to Chang 1 was deposited during the shrinkage phase of lacustrine basin [19, 20]. The peak of the expansion period is recorded in the Chang 7 member. During this stage, dark fine-grained shale and mudstone were deposited in semideep and deep lake settings, forming high-quality source rocks and reservoirs [21]. The study area is close to the depositional center of the lacustrine basin at this stage [22–24] and covered by the semideep and deep lake surfaces. The thickness of shale formation in this area ranges from 100 m to 135 m (Figure 2).

3. Materials and Methods

3.1. X-Ray Diffraction Analysis. The mineral composition of whole-rock has been identified by using X-ray diffraction analysis (XRD). Samples of the Chang 7 Formation from the Xiasiwan area of Ordos Basin were analyzed for whole-rock mineral composition using the D/MAX2500 X-ray diffractometer. Each sample was crushed and sieved to 200 mesh and fully dried. The angle range was 3-85° at the rate of 2θ for the whole-rock mineral analysis.

3.2. X-Ray Fluorescence Analysis. The X-ray fluorescence technique has been used to generate quantitative geochemical results for many years [25–29]. The implementation of the handheld XRF for elemental research can provide unique insights into the lithological analysis by measuring major elements with error less than 5% [30], such as silica (Si), aluminum (Al), iron (Fe), potassium (P), calcium (Ca), and magnesium (Mg). Samples from depths 1358 m to 1394 m in the Yanchang Formation in Well Y1 were measured at intervals of 0.1 m, and the lithology of the measuring points is shown in Figure 3. In order to ensure the accuracy of the measurement results, each sample was tested for up to 120 seconds, and each sample point is measured three times. The average value of each measurement was taken to analyze changes and distribution of the major elements from the shale in this shale layer.

4. Results

Based on core observations (Figure 4), the shale Yanchang Formation in the Well Y1 was measured from 1358 m to 1394 m. Lacustrine shale was controlled by climate and seasonal changes, which directly affected the density and thickness of laminated [31]. Moreover, the texture of lacustrine shale was sensitive to sediment environment, in turn leading to complicated laminated development. Hence, the density of laminated reflected vertical changes of lithofacies [32]. Then, we divided Well Y1 into ①~⑨ units on the basis of core observation (Table 1). Elemental measurement of these shale intervals reveals a total of 360 groups of major elements, and these were further characterized into distinct silty laminated shale and the argillaceous shale. Argillaceous shale was dark black with oily fresh surface. XRF results showed that argillaceous shale was mainly composed of Si, Al, and Fe, which consists of high clay content obtained from the XRD test. Silty laminated shale was interbed of dark shale and silt. The Si content of silty laminated shale was the highest among three types of shale, which also proved by high quartz and feldspar content. Calcareous laminated shale was black or gray black, consisting highest Ca content and lowest Al and K. XRD results indicated that calcite, dolomite, and pyrite were the highest in these three lithofacies.

4.1. Lithologic Characteristics of Chang 7. Through core observation, Chang 7 shale is mainly composed of argillaceous shale, silty laminated shale, and calcareous laminated shale (Figure 4). Argillaceous shale is characterized by high carbon content, thin flake, and well-developed foliation. Silty laminated shale is mainly light gray. The sandy lamina is straight, continuous, and vertically overlapping. Calcareous laminated shale is characterized by bright white calcareous lamina, clear

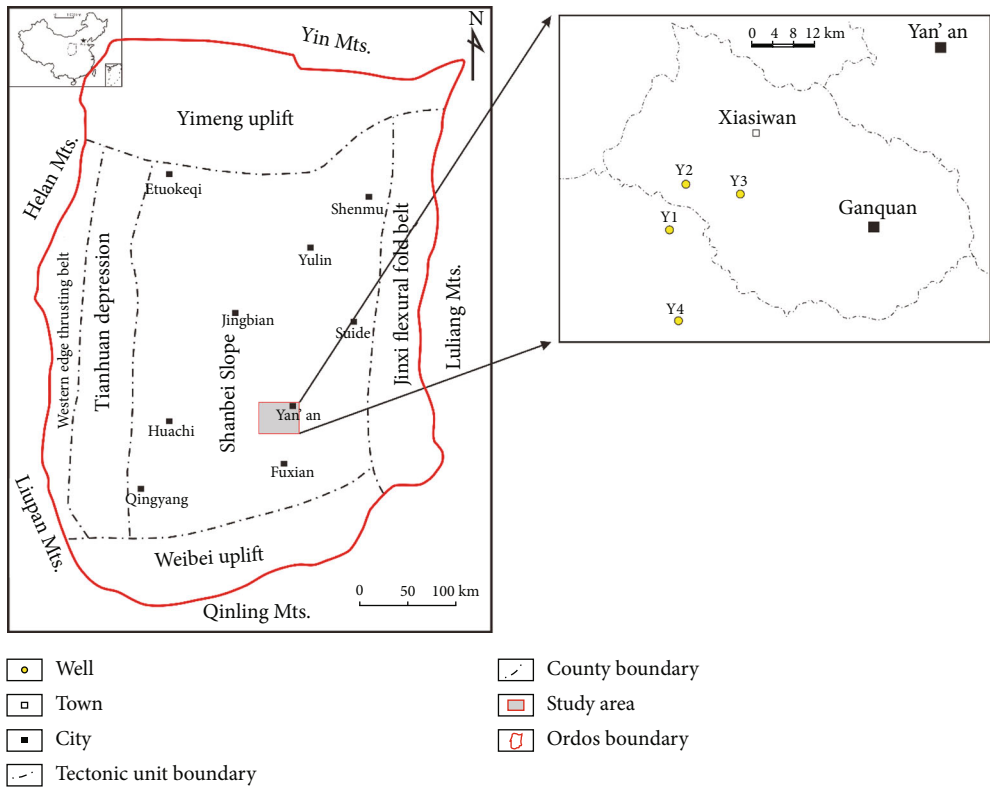

Figure 1: The location of Xiasiwan area in the tectonic units of Ordos Basin.

Series	Formation	Member	Thickness (m)	Lithology	Depositional environments
Upper Triassic	Yanchang	Chang 1	0 ~ 90		Swamp and shallow lacustrine
		Chang 2	0 ~ 140		Fluvial and delta
		Chang 3	0 ~ 135		
		Chang 4 + 5	90 ~ 100		Shallow lacustrine
		Chang 6	80 ~ 110		Delta
		Chang 7	100 ~ 135		Delta and deep lacustrine
		Chang 8	85 ~ 170		Delta and Shallow lacustrine
		Chang 9	90 ~ 120		
		Chang 10	50 ~ 400		Fluvial

Sandstone
Siltstone
Mudstone
Coal
Shale

Figure 2: Stratigraphy and lithology of Upper Triassic Yanchang Formation (modified after [3]).

(a)

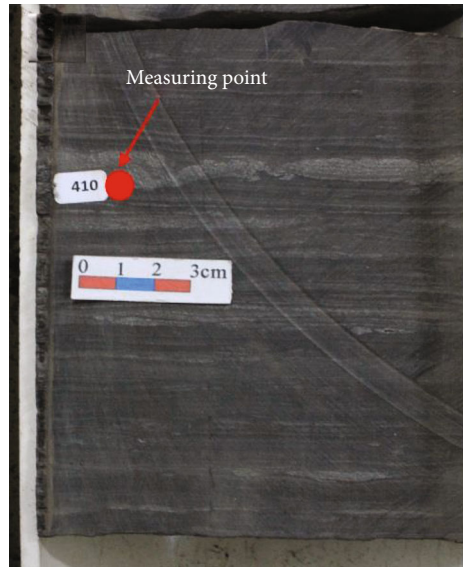

(b)

(c)

Figure 3: Major element test method.

boundary with shale, high brittleness, and easy to separate from shale.

4.2. Mineralogic Characteristics of Chang 7. X-ray diffraction analysis results from core samples show that the Chang 7 shale is composed of clay, quartz, feldspar, calcite, ankerite, siderite, and pyrite (Figure 5). Clay, quartz, and feldspar are main mineral composition. The mineral composition shows that argillaceous shale possesses higher content of clay mineral, with average values of 57.38%. The average contents of quartz and feldspar is 36.49% in argillaceous shale. Calcite, ankerite, siderite, and pyrite are merely lower than 5%. In silty laminated shales, quartz and feldspar are relatively high, with 57.38% in average, while the clay is significantly lower with proportion of 34.08%. The percentage of calcite and ankerite in calcareous laminated shale considerably larger than that of argillaceous shale and silty laminated shale, with the proportion of 25.33% and 10.7%, respectively, and calcareous laminated shale has a relatively lower content in terms of quartz and feldspar.

4.3. Element Composition Characteristics. The results show that the major elements the Chang 7 shale in this well are Si, Al, Fe, K, Ca, Mg, P, S, Ti, and Mn (Table 2), with Si, Al, and Fe with concentrations greater than 5%. The concentration of Si element was the highest, with a mathematical average of 26.36%. The concentration of Al on the other hand has an average 7.91%. While, the Fe in this shale has an average concentration of 5.04%. In addition to the above three main elements, there are also a minimal amount of K (1.9% average concentration), Ca (2.9% average concentration), Mg (1.02% average concentration), and S (0.91% average concentration). The average content of P, Ti, and Mn are less than

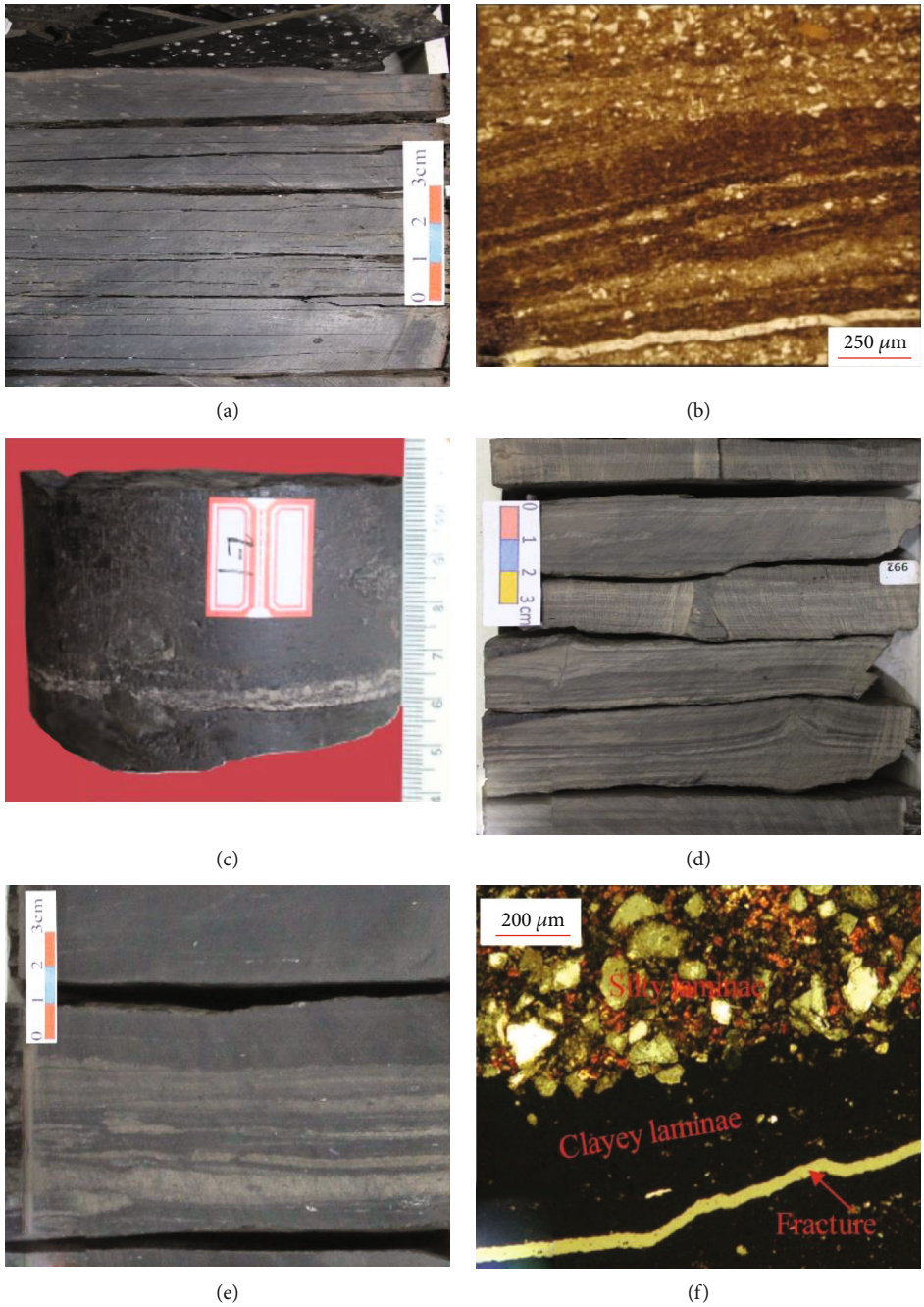

(a) (b) (c) (d) (e) (f)

Figure 4: Lithologic characteristics of shale layers in Chang 7, Xiasiwan area. (a) 1369.11 m black shale in Well Y1. (b) Silty laminated in Well Y1 1371.35 m, single polarized light. (c) 1362.00 m calcareous laminated in Well Y1. (d) 1370.8 m silty laminated in Well Y1. (e) 1393.87 m silty laminated in Well Y1. (f) 1393.87 m silty laminated in Well Y1, single polarized light.

Table 1: Laminated density classified standard of Y1 units.

Unit	①	②	③	④	⑤	⑥	⑦	⑧	⑨
Laminated density (no./m)	31~43	5 ~ 33	20~42	6	20~56	2	16~48	5 ~ 20	42~55

0.5%. Compared with the North American shales [26], the geochemical observations of Chang 7 shale are similar to that of North American shales as shown in Table 1. See Table 1 for min and max elemental concentration of the elements discussed.

We found that the element content closely related to mineral content from XRF and XRD results plots, e.g., Ca vs. calcite, K vs. feldspar, Si vs. quartz, and (Al+Si) vs. clay (Figure 6).

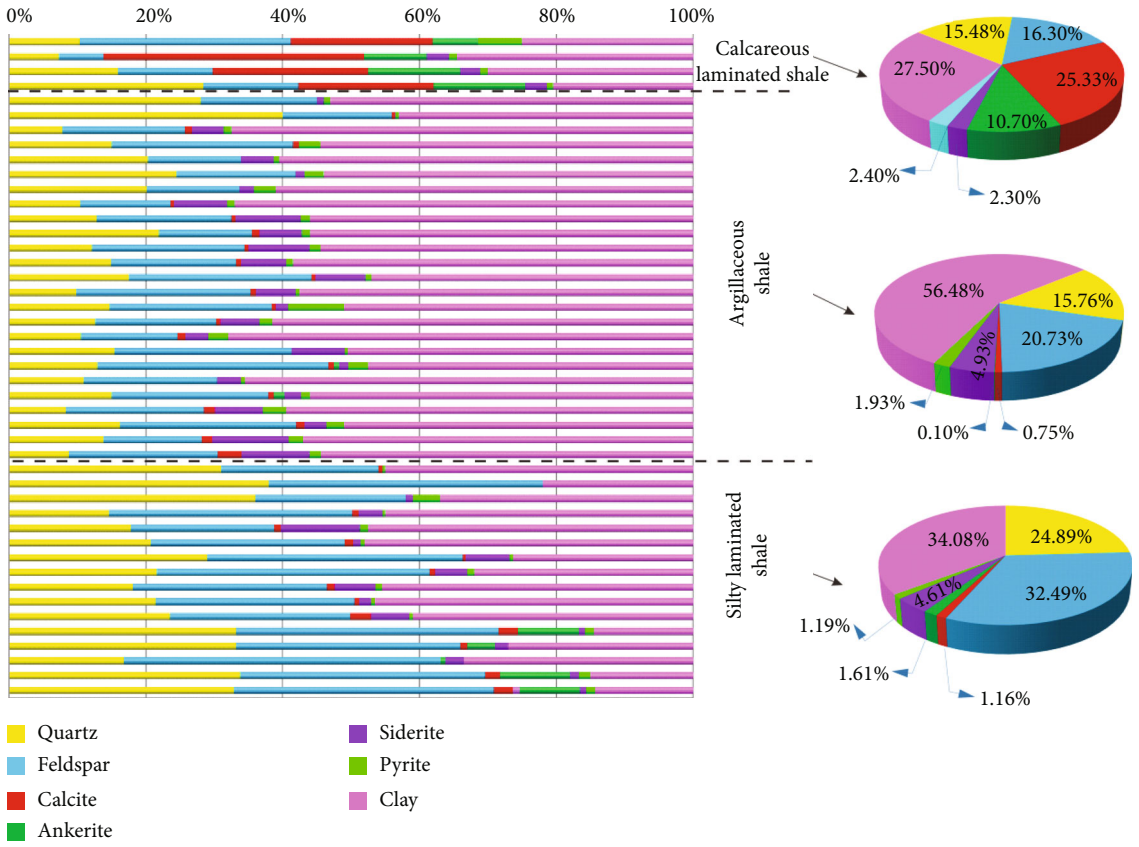

Figure 5: Mineral content of the studied area in Chang 7.

Table 2: North America Shale and Chang 7 Shale elemental concentrations.

Elements	North America shale								Chang 7 Shale		
	Woodford Fm		Barnett Fm		Ohio Shale		Eagle Ford Fm				
	Min	Max	Min	Max	Min	Max	Min	Max	Min	Max	Average
Si (%)	5.89	**38.2**	6.22	32.7	26.8	28.8	*3.75*	22.6	7.508	38.91	26.36
Al (%)	*0.64*	7.62	1.2	8.47	6.87	**10.77**	1.07	5.98	2.851	11.31	7.91
Fe (%)	0.61	**4.92**	0.64	3.54	3.09	4.6	*0.43*	3.57	1.72	13.81	5.04
K (%)	0.17	**3.51**	0.27	1.83	2.92	4.32	**0.14**	1.61	0.7	2.71	1.9
Ca (%)	*0.07*	18.1	2.77	**31.2**	0.19	0.71	9.36	34.7	0.32	24.07	2.02
Mg (%)	0.27	**10.25**	0.52	2.64	0.66	1.08	*0.24*	0.66	0.33	4.49	1.02
S (%)	0.46	**5.32**	*0.25*	2.24	0.72	2.25	0.33	3.81	0.026	5.024	0.91
P (%)	*0.01*	0.48	0.07	**0.98**	0.02	0.17	0.02	0.15	0.047	0.94	0.217
Ti (%)	0.04	0.33	0.07	0.46	0.4	**0.53**	*0.04*	0.39	0.083	0.575	0.42
Mn (%)	*0.008*	**0.325**	0.008	0.031	0.008	0.031	0.008	0.023	0.011	0.355	0.09

*Bold and italic are the maximum and minimum values of this element, respectively.

5. Discussion

5.1. Elemental Distribution across Chang 7 Unit. Based on the observed lithologic changes and the distribution characteristics of silty laminated in cores in the Chang 7 (units ①~⑨ Figure 7) of Well Y1, the elemental differences in each stratigraphic unit was recorded and described in sections. The frequency of occurrence of silty laminated is relatively large in units ①, ③, ⑤, ⑦, and ⑨ units (in the upper, middle, and lower shale layers) in this Well (see Figure 7). These shales contain mainly between 16 counts and 56 counts per meter. The frequency of occurrence of silty laminated in upper ②, middle ④ and ⑥, and lower ⑧ shale units is relatively low, mainly between 5 counts per meter and 18 counts per meter.

The elemental composition in each unit was counted, respectively (Table 3), and the results show that units ①, ③,

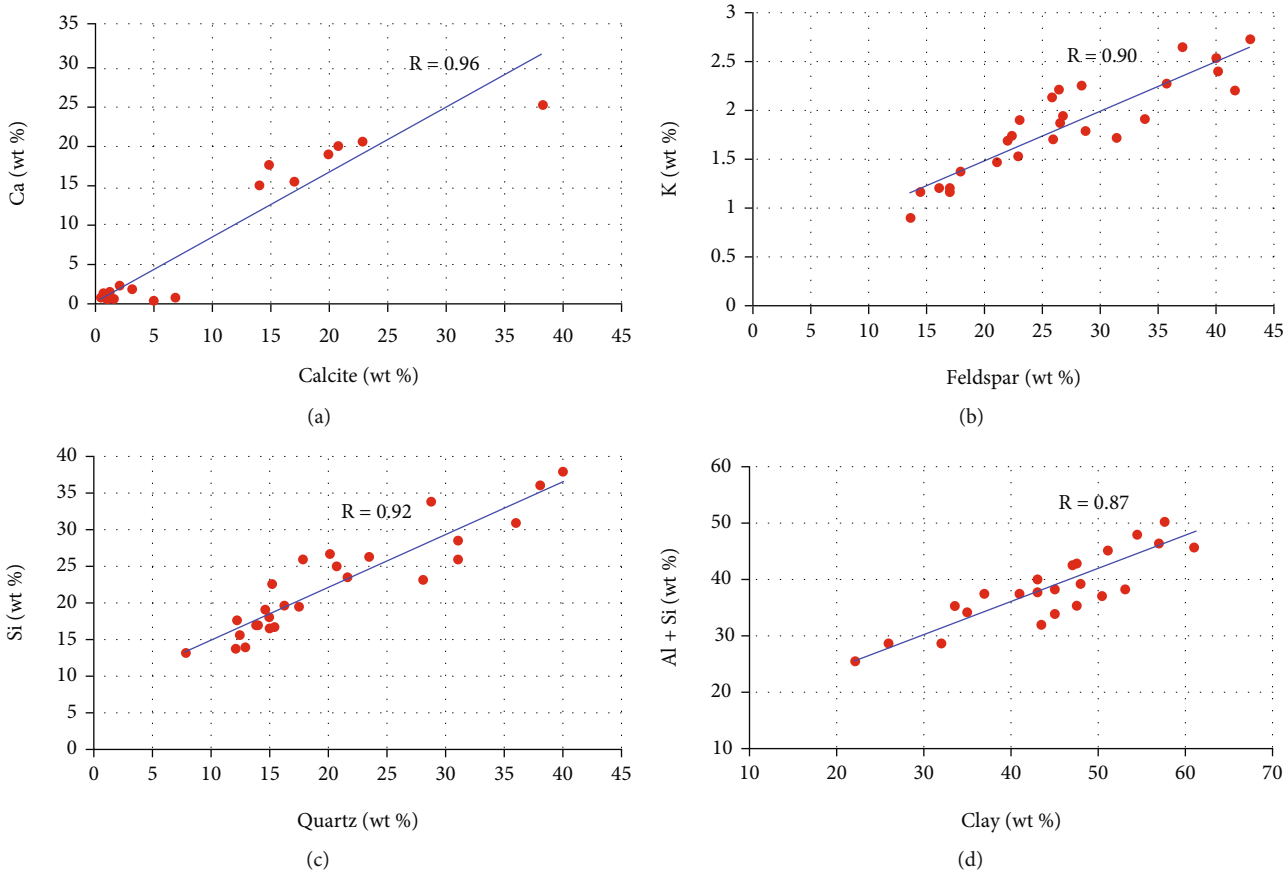

Figure 6: The plots of element content and mineral content.

⑤ (Figures 4(b) and 4(d)), ⑦, and ⑨ (Figures 4(e) and 4(f)), where the silty lamination is relatively dense has higher silica content, with Si values between 2.93% and approximately 38.91%. In these units, the concentration of aluminum (Al), iron (Fe), and potassium (K) is relatively low with respective values between 0.53% and approximately 10.73% for Al, 1.72%~10.10% for Fe, and 0.70%~2.51% for K. However, in units ②, ④ (Figure 4(a)), ⑥, and ⑧ with relatively lower silty lamina densities, the content of Si is relatively low, with values ranging from 11.87% to approximately 30.20%, while the content of Al, Fe, and K is relatively higher, with values 4.13%~10.63%, 3.76%~13.81%, and 0.92%~2.71%, respectively. The contents of Ca and Mg are relatively low, except for the extremely high values in ② (Figure 4(c)), ③, ⑤, ⑦, and ⑧ units.

Sedimentary rocks are the materials formed response to sedimentary environments, which is thus composed of different minerals and elements. Therefore, stratigraphic change in elemental composition implies that the sedimentary environment has slight changes during the deposition of Chang 7 shale. The unit with higher silica may be due to the relatively shallow water depth during the deposition or the inflow of a relatively large volume of water which carried siliceous debris to a deeper part s of the basin. The unit with higher concentration of Ca and Mg is due to the evolution of organic matter to form acids, and with further evolution, acid decarboxyl group to form hydrocarbons and carbonate ions. These carbonate ions combine with Ca and Mg in water to form calcite and dolomite [9, 33–35]. Ca/Mg values can reflect climates humidity due to the varied solubility [36–38]. Calcareous laminated shale with high Ca/Mg value demonstrated dryer climate compared to other two lithofacies. Argillaceous shale showed lower Si/Al value, which can character grain size to deduce water depth [39, 40]. We thus concluded that argillaceous shale developed in deep lake. Silty laminated shale with lowest Fe content indicated that it was deposited in oxidizing environment.

The abundance of Si, Al, Fe, K, Ca, Mg, and other elements were calculated according to three lithologies, identified from drilled core and thin section analysis. These are argillaceous shales, silty laminated shales, and calcareous laminated shales. The elemental composition in the Y1 shale unit (Table 4) shows that the presence of Silica is highest in this shale, with values ranging from 14.25% to 34.17%. The contents of Al, Fe, K, and Ca were 4.12% to 11.31%, 2.48% to 13.81%, 1.14% to 2.71%, and 0.32% to 7.80%, respectively. The concentration of Mg element was the lowest in the unit, with the range between 0.33% and 1.75%.

In the silty laminated shales, Si content is the highest, which ranges from 18.30% to 38.91%. The abundance of Al, Fe, K, and Ca are 3.71% to 10.25%, 1.72% to 7.32%, 0.59% to 2.46%, and 0.51% to 7.57%, respectively. The distribution of Mg was the lowest, with 0.47% to 1.90%. On the other hand, the calcareous laminated shales have higher relative abundance of Ca, with values from 8.95% to 24.07%,

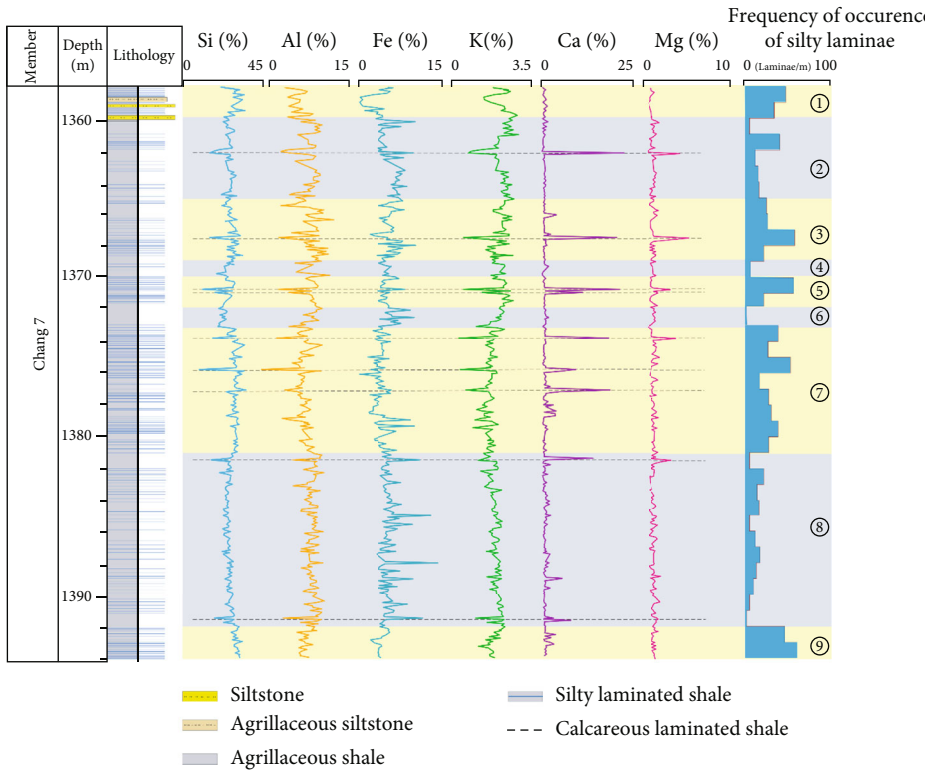

Figure 7: Lithology and element content of shale strata in Well Y1.

Table 3: Element contents of shale layers ① ~ ⑨ in Well Y1.

	Si (%)	Al (%)	Fe (%)	K (%)	Ca (%)	Mg (%)
①	26.84~38.91	5.18~9.02	1.72~5.67	1.47~2.38	0.54~1.36	0.71~1.05
②	11.87~30.20	4.13~10.16	3.76~9.98	0.92~2.71	0.32~24.07	0.33~3.57
③	7.58~30.55	2.93~10.73	2.87~10.03	0.74~2.51	0.70~22.18	0.61~4.49
④	17.16~21.24	5.57~11.31	4.32~6.30	1.78~2.51	0.44~1.27	0.67~1.23
⑤	9.96~30.03	2.58~8.68	2.87~7.23	0.73~2.42	0.63~21.87	0.62~2.62
⑥	17.16~22.56	4.47~9.57	4.55~9.81	1.69~2.55	0.59~1.43	0.36~1.19
⑦	2.93~32.41	0.53~9.61	2.76~10.10	0.70~1.95	0.66~17.75	0.47~3.15
⑧	14.5 ~ 29.76	4.55~10.63	3.77~13.81	1.14~2.22	0.51~7.80	0.52~2.71
⑨	25.37~31.72	6.06~9.19	3.14~4.85	0.91~1.81	0.62~3.65	0.67~1.22

Table 4: Element concentration of three types of lithology.

	Si (%)	Al (%)	Fe (%)	K (%)	Ca (%)	Mg (%)
Argillaceous shale	14.25~34.17	4.12~11.31	2.48~13.81	1.14~2.71	0.32~7.80	0.33~1.75
Silty laminated shale	18.30~38.91	3.71~10.25	1.72~7.32	0.59~2.46	0.51~7.57	0.47~1.90
Calcareous laminated shale	2.93~18.54	0.53~5.40	3.26~9.65	0.70~1.94	8.95~24.07	1.35~4.49

followed by Si, Al, Fe, and Mg, which range from 2.93% to 18.54%, 0.53% to 5.40%, 3.26% to 9.65%, and 1.35% to 4.49%, respectively. Also, the abundance of potassium is the lower with values between 0.70% and 1.94%. It can be observed that there are differences in the concentration of various elements in distinct lithologies in these shale layers. In consequence, the visual discrimination of the encountered shales in the Well Y1 can be attributed to the differences in these elemental compositions.

5.2. Standard for Fine Scale Lithology Identification. Based on the above analysis, we propose a criterion for lithology identification in shale layers with Si, Al, and Ca, which is sensitive to calcareous laminated shale. According to the ternary diagram of relative percentages of Si, Al, and Ca (Figure 8(a)), the content of Ca in calcareous laminated shale is obviously higher than that in argillaceous shale and silty laminated shale. Silty laminated shales contain relatively more Si element, while

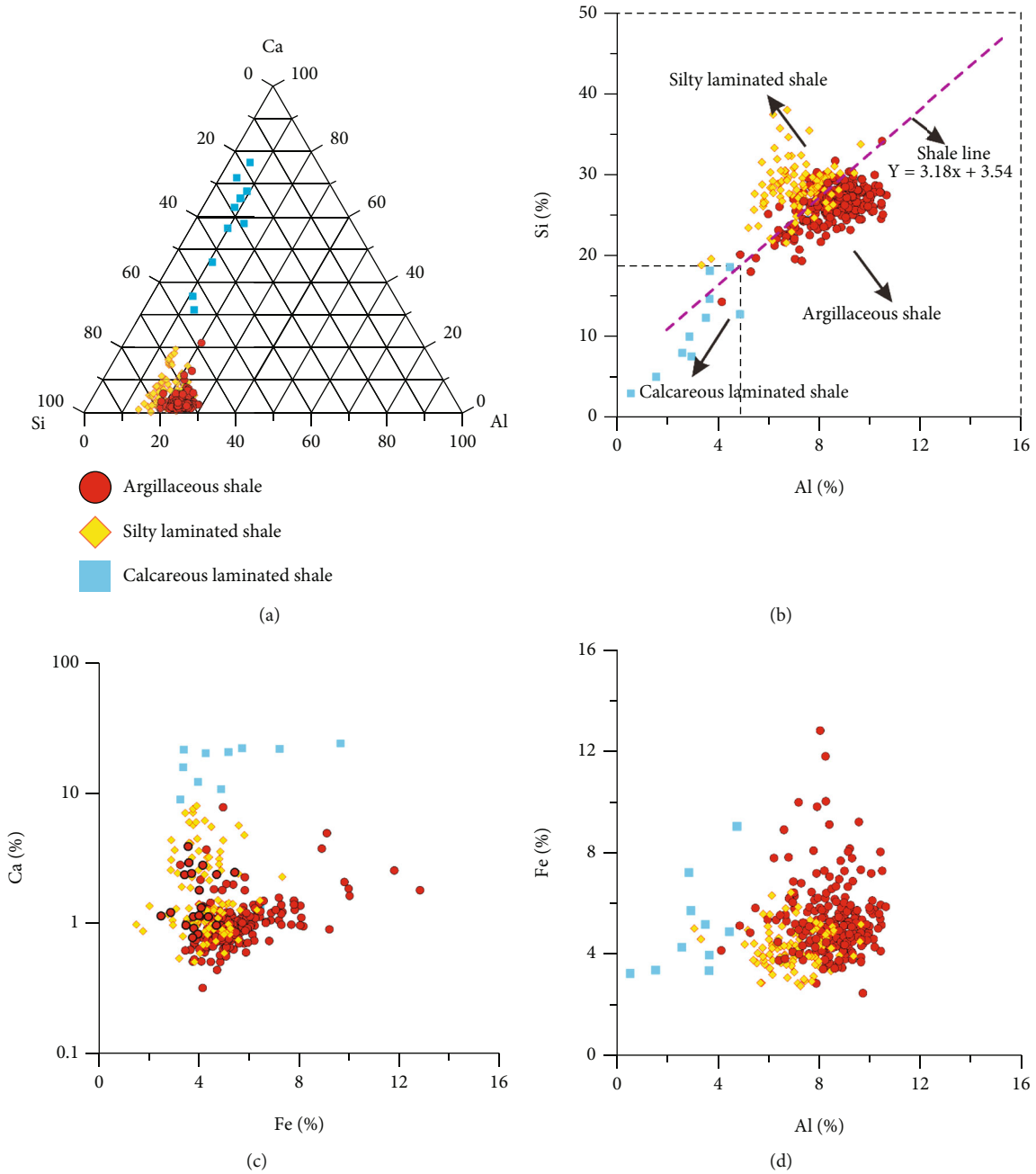

Figure 8: Element content relationship of different lithologies in Well Y1.

argillaceous shales contain a relatively higher Al element. However, the boundary between Ca and Al is not obvious in the ternary diagram. Cross-plot of Si and Al content (Figure 8(b)) shows that the content of Si and Al in argillaceous shale presents a linear relationship (shale line). Silty laminated shale plots above the shale line, and its Si content is relatively high. Using the shale line as the boundary, while argillaceous shale plots mainly below this line. The third type, the calcareous laminated shales, which are characterized by lower Si and Al content, thus plots in the lower quadrant of this plot.

In calcareous laminated shales, the concentration of Ca and Mg is relatively high, while the values of Si and Al is relatively low. Due to the influence of high concentration of Ca, Si, and Al is diluted to a large extent. Calcareous laminated shale has relatively high Ca content (>8.95%) (Figure 8(c)), and Al content is less than 4.49% (Figure 8(d)). However, there is no significant difference between identifying argillaceous shale from silty laminated shale. Therefore, we used the shale line as a boundary (Figure 8(b)). Lithology interpretation for points which lie above shale line is identified as silty laminated shale; while the points below the shale line with Ca element content greater than 8.95% identified as calcareous shales. Also, in this case, the rest of data represent argillaceous shales. Based on this, a criterion for lithologic identification from elemental logging in shale layers is proposed.

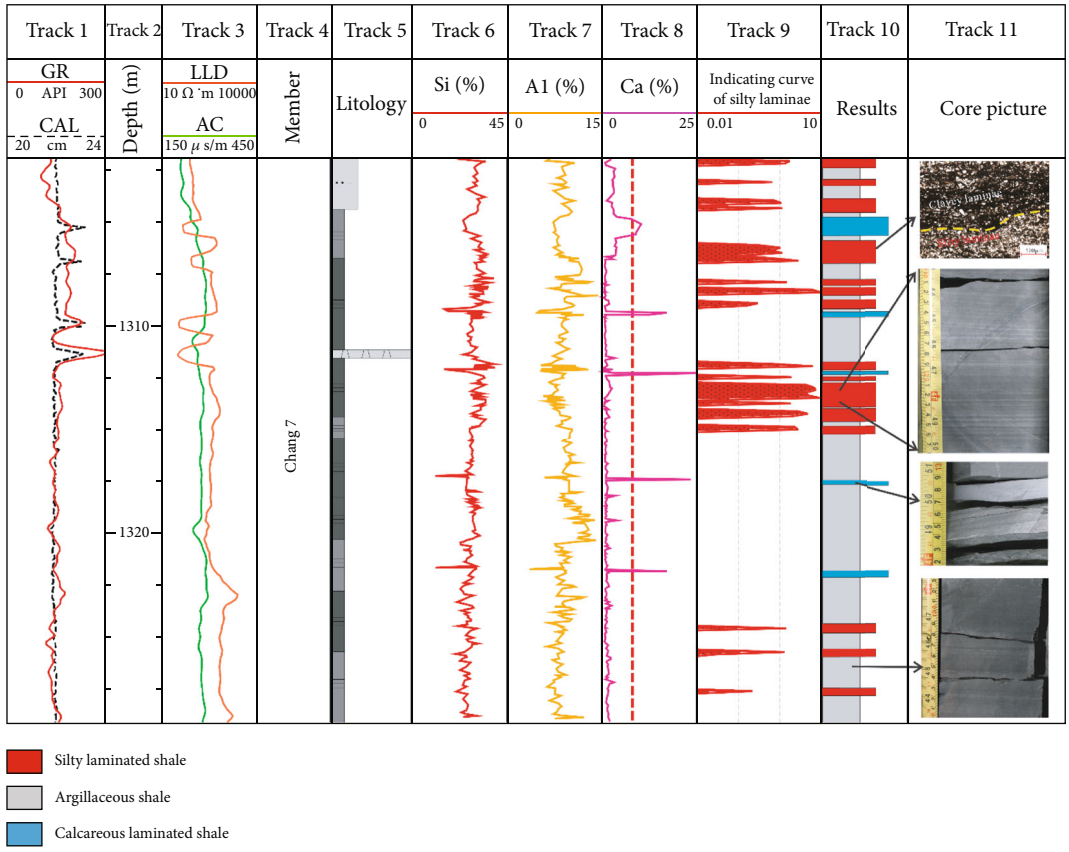

Figure 9: Identification results of silty laminated shale in Well Y2.

5.3. Validation of Lithology Identification. Based on the identification criteria described in this paper, the lithology of Chang 7 shale unit in Well Y2 was identified (Figure 9). The thickness of silty laminated shale in the well is between 0.33 m and 4.8 m (track 10 on the Figure 9). Calcareous laminated shale (track 10 on the Figure 9) is scattered throughout the shale series and are usually in thin laminated; the uncharacterized shale here is referred to as argillaceous shale.

The silty laminated shale is interbedded with gray or white silty laminated and black-gray shale. Under single polarized light, the light and dark layers are interbedded with the dark parts comprising of fine particle size, while the light layer comprises the coarser particle size. The results were validated with the thin section and drill cores and showed good agreement with the predicted lithology, while the core observation suggested silty laminated shales in depth (1312.9 ~ 1313.13 m), which is also consistent with the predicted results, thus indicating that the identification criteria established by XRF can be used to identify different suites of shales within a formation.

6. Conclusion

(1) The elemental make up of shale layers varies greatly, and there are differences among different lithologies; the content of Fe, Al, and other elements in shale is relatively high, with Fe ranging from 2.48% to 13.81% and Al from 4.12% to 11.31% in the study well. Silty laminated shale is characterized by high abundance of Si, ranging from 18.30% to 38.91%. Calcareous laminated shale on the other hand has relatively high concentration of Ca and Mg, ranging from 8.95% to 24.07% and Mg ranging from 1.35% to 4.49%, respectively

(2) Based on the abundance of elements Si, Al, Fe, and Ca in shale layers, the lithology identification standard of shales was established. Taking the shale line as the boundary, lithologies with Si content above the shale line is interpreted as silty laminated shale, while the lithologies with Ca abundance greater than 8.95% and plots below the shale line is interpreted as calcareous laminated shale, the rest of data represent argillaceous shales

(3) A test from Well Y2 shows that silty laminated shale, calcareous laminated shale, and argillaceous shale can be predicted by the lithologic identification criteria described, and the identification results are in good agreement with thin section analysis and visual identification from drilled core

Data Availability

Data are available upon request to the corresponding author's email address: amelia-yu@hotmail.com.

Conflicts of Interest

The authors declare that they have no competing interests.

Acknowledgments

This work was jointly funded by the National Natural Science Foundation of China (41902145), Natural Science Basic Research Plan in Shaanxi Province of China (2020JQ-594), Young researcher of science and technology and foreign expert service plan in Shaanxi Province (2021KJXX-28, 2021JZY-016), and Changqing Oilfield, PetroChina (ZDZX2021-05).

References

[1] A. Aplin and J. Macquaker, "Mudstone diversity: origin and implications for source, seal, and reservoir properties in petroleum systems," *AAPG Bulletin*, vol. 95, no. 12, pp. 2031–2059, 2011.

[2] K. Liu, L. Wang, M. Ostadhassan, J. Zou, B. Bubach, and R. Rezaee, "Nanopore structure comparison between shale oil and shale gas: examples from the Bakken and Longmaxi formations," *Petroleum Science*, vol. 16, no. 1, article 277, pp. 77–93, 2019.

[3] Y. Yuan, R. Rezaee, E. Al-Khdheeawi et al., "Impact of composition on pore structure properties in shale: implications for micro-/mesopore volume and surface area prediction," *Energy & Fuels*, vol. 33, no. 10, pp. 9619–9628, 2019.

[4] J. Chermak and M. Schreiber, "Mineralogy and trace element geochemistry of gas shales in the United States: environmental implications," *International Journal of Coal Geology*, vol. 126, article S0166516213002723, pp. 32–44, 2014.

[5] J. Rimstidt, J. Chermak, and M. Schreiber, "Processes that control mineral and element abundances in shales," *Earth-Science Reviews*, vol. 171, article S0012825216302860, pp. 383–399, 2017.

[6] Y. Yuan, R. Rezaee, H. Yu, J. Zou, K. Liu, and Y. Zhang, "Compositional controls on nanopore structure in different shale lithofacies: a comparison with pure clays and isolated kerogens," *Fuel*, vol. 303, article S0016236121009583, p. 121079, 2021.

[7] J. Du, L. Hu, J. Meegoda, and G. Zhang, "Shale softening: observations, phenomenological behavior, and mechanisms," *Applied Clay Science*, vol. 161, article S0169131718301935, pp. 290–300, 2018.

[8] D. Ross and R. Bustin, "The importance of shale composition and pore structure upon gas storage potential of shale gas reservoirs," *Marine and Petroleum Geology*, vol. 26, no. 6, article S0264817208001153, pp. 916–927, 2009.

[9] J. Yin, C. Gao, M. Zhu et al., "Oil accumulation model and its main controlling factors in Lower Yanchang Formation, Wuqi-Dingbian area, Ordos Basin, China," *Geofluids*, vol. 2021, Article ID 5511563, 10 pages, 2021.

[10] M. Raji, D. Gröcke, H. Greenwell, J. Gluyas, and C. Cornford, "The effect of interbedding on shale reservoir properties," *Marine and Petroleum Geology*, vol. 67, article S0264817215001439, pp. 154–169, 2015.

[11] M. Arif, M. Mahmoud, Y. Zhang, and S. Iglauer, "X-ray tomography imaging of shale microstructures: a review in the context of multiscale correlative imaging," *International Journal of Coal Geology*, vol. 233, article S0166516220306376, p. 103641, 2021.

[12] H. Dong, Y. Zhang, M. Lebedev, M. Arif, Y. Yuan, and S. Iglauer, "Simulating coal permeability change as a function of effective stress using a microscale digital rock model," *Energy & Fuels*, vol. 35, no. 10, pp. 8756–8762, 2021.

[13] H. Yu, Z. Wang, R. Rezaee et al., "Applications of nuclear magnetic resonance (NMR) logs in shale gas reservoirs for pore size distribution evaluation," in *SPE/AAPG/SEG Unconventional Resources Technology Conference*, One Petro, 2017.

[14] H. Yu, Y. Zhang, M. Lebedev et al., "X-ray micro-computed tomography and ultrasonic velocity analysis of fractured shale as a function of effective stress," *Marine and Petroleum Geology*, vol. 110, article S0264817219303253, pp. 472–482, 2019.

[15] B. Liu, H. Wang, X. Fu et al., "Lithofacies and depositional setting of a highly prospective lacustrine shale oil succession from the Upper Cretaceous Qingshankou Formation in the Gulong sag, northern Songliao Basin, northeast China," *AAPG Bulletin*, vol. 103, no. 2, pp. 405–432, 2019.

[16] M. Arif, Y. Zhang, and S. Iglauer, "Shale wettability: data sets, challenges, and outlook," *Energy & Fuels*, vol. 35, no. 4, pp. 2965–2980, 2021.

[17] B. Liu, Y. Lu, Y. Meng, X. Li, X. Gao, and Q. Ma, "Petrologic characteristics and genetic model of lacustrine lamellar fine-grained rock and its significance for shale oil exploration: a case study of Permian Lucaogou Formation in Malang sag, Santanghu Basin, NW China," *Petroleum Exploration and Development*, vol. 42, no. 5, article S1876380415300604, pp. 656–666, 2015.

[18] J. Zhao, N. Mountney, C. Liu, H. Qu, and J. Lin, "Outcrop architecture of a fluvio-lacustrine succession: upper Triassic Yanchang Formation, Ordos Basin, China," *Marine and Petroleum Geology*, vol. 68, article S0264817215300891, pp. 394–413, 2015.

[19] L. Xiao, Z. Li, Y. Hou, L. Xu, L. Wang, and Y. Yang, "Characteristics of organic macerals and their influence on hydrocarbon generation and storage: a case study of continental shale of the Yanchang Formation from the Ordos Basin, China," *Geofluids*, vol. 2021, Article ID 5537154, 17 pages, 2021.

[20] H. Guo, W. Jia, P. Peng et al., "The composition and its impact on the methane sorption of lacustrine shales from the Upper Triassic Yanchang Formation, Ordos Basin, China," *Marine and Petroleum Geology*, vol. 57, article S026481721400186X, pp. 509–520, 2014.

[21] J. Fu, S. Li, L. Xu, and X. Niu, "Paleo-sedimentary environmental restoration and its significance of Chang 7 member of triassic Yanchang formation in Ordos Basin, NW China," *Petroleum Exploration and Development*, vol. 45, no. 6, article S1876380418301046, pp. 998–1008, 2018.

[22] Y. Yang, W. Li, and L. Ma, "Tectonic and stratigraphic controls of hydrocarbon systems in the Ordos basin: a multicycle cratonic basin in Central China," *AAPG Bulletin*, vol. 89, no. 2, pp. 255–269, 2005.

[23] L. Zeng and X. Li, "Fractures in sandstone reservoirs with ultra-low permeability: a case study of the Upper Triassic Yanchang Formation in the Ordos Basin, China," *AAPG Bulletin*, vol. 93, no. 4, pp. 461–477, 2009.

[24] X. Yuan, S. Lin, Q. Liu et al., "Lacustrine fine-grained sedimentary features and organicrich shale distribution pattern: a case study of Chang 7 Member of Triassic Yanchang Formation in Ordos Basin, NW China," *Petroleum Exploration and Development*, vol. 42, no. 1, article S1876380415600040, pp. 37–47, 2015.

[25] H. Rowe, N. Hughes, and K. Robinson, "The quantification and application of handheld energy-dispersive x-ray fluorescence (ED-XRF) in mudrock chemostratigraphy and geochemistry," *Chemical Geology*, vol. 324-325, pp. 122–131, 2012.

[26] S. Lim, T. Murphy, K. Wilson, and K. Irvine, "Leaded paint in Cambodia—pilot-scale assessment," *Journal of Health and Pollution*, vol. 5, no. 9, pp. 18–24, 2015.

[27] G. Hall, G. Bonham-Carter, and A. Buchar, "Evaluation of portable X-ray fluorescence (pXRF) in exploration and mining: phase 1, control reference materials," *Geochemistry: Exploration, Environment, Analysis*, vol. 14, no. 2, pp. 99–123, 2014.

[28] D. Li, R. Li, Z. Zhu et al., "Rare earth elements geochemistry characteristics and their geological implications of lacustrine oil shale from Chang 7 oil layer in southern Ordos Basin, China," *Geological Journal*, vol. 52, pp. 119–131, 2017.

[29] B. Liu, Y. Song, K. Zhu, P. Su, X. Ye, and W. Zhao, "Mineralogy and element geochemistry of salinized lacustrine organic-rich shale in the Middle Permian Santanghu Basin: implications for paleoenvironment, provenance, tectonic setting and shale oil potential," *Marine and Petroleum Geology*, vol. 120, article S0264817220303524, p. 104569, 2020.

[30] H. Cao, H. Wang, and R. Zhao, "The application of the handheld energy-dispersive X-ray fluorescence (ED-XRF) in the cyclostratigraphy research-a case study from the Xiaogou formation of the lower cretaceous in the Qingxi Sag, Jiuquan Basin," *Earth Science*, vol. 42, no. 12, pp. 2299–2311, 2017.

[31] O. Lazar, K. Bohacs, J. Macquaker, J. Schieber, and T. Demko, "Capturing key attributes of fine-grained sedimentary rocks in outcrops, cores, and thin sections: nomenclature and description guidelines," *Journal of Sedimentary Research*, vol. 85, no. 3, pp. 230–246, 2015.

[32] T. Zhang, S. Hu, Q. Bu et al., "Effects of lacustrine depositional sequences on organic matter enrichment in the Chang 7 Shale, Ordos Basin, China," *Marine and Petroleum Geology*, vol. 124, article S0264817220305614, p. 104778, 2021.

[33] R. Zhu, J. Cui, Z. Luo, Z. Mao, K. Xi, and L. Su, "A discussion on the genesis of carbonate concretions in the Chang 7 Member of the Middle-Upper Triassic Yanchang Formation of Ordos basin," *Acta Geologica Sinica*, vol. 95, no. 11, pp. 3442–3454, 2020.

[34] W. Li and S. Li, "Review on the high-resolution varved lake sediments as a proxy of paleoenvironment," *Advances in Earth Science*, vol. 14, no. 2, p. 172, 1999.

[35] G. Wang, "Laminae combination and genetic classification of Eogene shale in Jiyang Depression," *Journal of Jilin University (Earth Science Edition)*, vol. 42, no. 3, pp. 666–680, 2012.

[36] P. Wignall and R. Twitchett, "Oceanic anoxia and the end Permian mass extinction," *Science*, vol. 272, no. 5265, pp. 1155–1158, 1996.

[37] M. Adabi, M. Salehi, and A. Ghabeishavi, "Depositional environment, sequence stratigraphy and geochemistry of Lower Cretaceous carbonates (Fahliyan Formation), south-west Iran," *Journal of Asian Earth Sciences*, vol. 39, no. 3, article S1367912010000891, pp. 148–160, 2010.

[38] J. Hu, W. Yang, S. Li et al., "Trace element and isotope (C, S, Sr, Nd, Fe) geochemistry constraints on the sedimentary environment of the early Neoproterozoic Shilu BIF and associated dolostones, South China," *Precambrian Research*, vol. 372, article S0301926822000547, p. 106610, 2022.

[39] M. Caetano, R. Prego, C. Vale, H. Pablo, and J. Marmolejo-Rodríguez, "Record of diagenesis of rare earth elements and other metals in a transitional sedimentary environment," *Marine Chemistry*, vol. 116, no. 1-4, article S0304420309001273, pp. 36–46, 2009.

[40] M. Yalcin, D. Nyamsari, O. Ozer Atakoglu, and F. Yalcin, "Chemical and statistical characterization of beach sand sediments: implication for natural and anthropogenic origin and paleo-environment," *International journal of Environmental Science and Technology*, vol. 19, no. 3, article 3280, pp. 1335–1356, 2022.